Hydrol. Earth Syst. Sci. Discuss., 3, 395–425, 2006
www.hydrol-earth-syst-sci-discuss.net/3/395/2006/

Hydrology and Earth System Sciences Discussions

Papers published in *Hydrology and Earth System Sciences Discussions* are under open-access review for the journal *Hydrology and Earth System Sciences*

A new method for determination of Most Likely Initiation Points and the evaluation of Digital Terrain Model scale in terrain stability mapping

P. Tarolli[1] **and D. G. Tarboton**[2]

[1]Department of Land and Agroforest Environments, AGRIPOLIS, University of Padova, 35020 Legnaro, Padova, Italy
[2]Department of Civil and Environmental Engineering, Utah State University, Logan, Utah, USA

Received: 10 January 2006 – Accepted: 14 February 2006 – Published: 6 April 2006

Correspondence to: P. Tarolli (paolo.tarolli@unipd.it)

Abstract

Physically-based models have been used previously to map areas of potential instability where shallow landslides may initiate. Here we introduce a new approach for determining the Most Likely Initiation Points (MLIP) for landslides. We identify the location with critical (lowest) stability index from a terrain stability model on each downslope path from ridge to valley. The SINMAP Stability Index (SI) was applied with this method. Only potential initiation points less than a threshold are considered to avoid identification of stable locations on downslope paths that do not contain any unstable locations. Mapped or observed landslides are often used to evaluate the effectiveness of model derived terrain stability maps, but a problem with these observations is that they may demarcate the entire landslide scar, including run out zones, rather than just initiation locations. Comparing such observations to SI does not provide a meaningful way to assess the effectiveness of the SI map because the demarcated area may include considerable area with stable SI values. In this paper we suggest using the relative density of MLIP locations within and outside demarcated landslide areas to assess the discriminating capability of a SI map. This approach was tested using landslides mapped from aerial photographs and airborne laser altimetry (LIDAR) derived elevation data for a small basin located in the Northeastern Region of Italy. Digital Terrain Models (DTMs) were derived from the LIDAR data for a range of grid cell sizes (from 2 to 50 m) and SI and MLIP evaluated for each. We found that the direct comparison of SI within and outside of landslides was not effective. However when MLIP was used we found appreciable differences between the density of MLIP points within and outside mapped landslides with ratios as large as three or more with the highest ratios for a DTM grid cell size of 10 m. This demonstrated the utility of the MLIP approach to quantifying the effectiveness of a terrain stability map when comparisons are to mapped landslides that include runout zones. This also suggests that in this study area, where landslides occurred in complexes that were sometimes more than 100 m wide, a DTM scale of 10 m is optimal. DTM scales larger than 10 m result in loss of resolution, while for DTM

HESSD

3, 395–425, 2006

scales smaller than 10 m the physical processes responsible for triggering landslides are obscured by smaller scale DTM variability that is resolved.

1 Introduction

Landsliding associated with rainstorms is a major process of landscape evolution on steep hillslopes. Shallow landsliding in steep, soil-mantled landscapes can generate debris flows which scour low-order channels, deposit large quantities of sediment in higher order channels and pose a significant hazard. The hazard occurs where development has encroached on debris flow source and run-out areas. A variety of approaches are available to assess landslide hazard and produce maps portraying its spatial distribution (landslide hazard mapping). In the last decade, process-based theories and models have been developed that represent the essential processes controlling shallow landsliding, yet remain simple enough that they can be calibrated and validated using observed landslides inventories. Many of these Terrain Stability Models (TSMs) are based upon the infinite slope stability model (e.g. Hammond et al., 1992; Montgomery and Dietrich, 1994; Wu and Sidle, 1995). Dietrich et al. (1992) and Montgomery and Dietrich (1994) developed a simple physically based model based on digital terrain data, which couples a shallow steady state saturated subsurface flow model with an infinite slope stability model. The model is based on the assumptions that shallow subsurface flow dictates the pore pressure field and that steady state flow mimics the spatial pattern of soil pore pressures during transient storms and can be used to map the relative potential for shallow landsliding across a landscape. Pack et al. (1998) introduced a stability index mapping approach (SINMAP) to terrain stability mapping, a methodology based upon the same concept as Montgomery and Dietrich (1994) in that it combines steady-state hydrologic concepts with the infinite slope stability model. Nevertheless some aspect are different: a) grid-based rather than contour-based Digital Terrain Model (DTM) methodology is used following the work of Tarboton (1997); b) cohesion is retained in the infinite slope stability model to account for soil

cohesion or root strength; c) parameter uncertainty is incorporated through the use of uniform probability distributions for uncertain parameters.

The accuracy of procedures relying on process-based theories depends on the quality of topographic data and is limited by the underlying assumptions used in the models, which cannot account for many factors which are known to influence landslide hazard, such as mechanically weak rocks, springs, locally high or low root strength and soil thickness, to name a few. With respect to the quality, and resolution of topographic data the accuracy of base point survey data and the method used to interpolate the Digital Terrain Model from point survey data can influence the results of TSMs. New survey techniques have been introduced in the last few years; an example of these is the use of laser sensors on aircraft (Akermann, 1999; Kraus and Pfeifer, 2001; Briese, 2004). This technology, called LIDAR (LIght Detection And Ranging), provides high quality digital terrain data, and provides more information about land cover than was previously available. The application of airborne laser altimetry technology to slope stability modeling has the potential to improve model performance and benefit land management.

There may be some limitations to the improvement of landslide modeling which can be achieved by using very fine topographic data. Regardless of the algorithms or type of DTM used, all DTM analyses depend crucially on the assumption that the flow pathways will be predominantly controlled by the surface topography of the catchment. Even in shallow systems, the bedrock topography may have a greater control on downslope saturated flow than the surface topography. It is likely that differences between surface and bedrock topography is relatively greater at very fine DTM resolution; therefore, very fine topographic data may lose representativeness, at least for the modeling of subsurface flow. Practical limits on LIDAR accuracy are still being defined (McKean and Roering, 2004). Data errors can be described as those originating from the hardware/software components of the LIDAR system, those related to the mission design and conduct, and those associated with the laser target characteristics (e.g. topography and vegetation contamination in the distribution of lidar elevation data points)

HESSD
3, 395–425, 2006

(McKean and Roering, 2004).

In this paper we present a new method for determining the Most Likely Initiation Points (MLIP) where landslides may initiate. The method identifies the grid cell with critical (lowest) stability index on each downslope path from ridge to valley. Only potential initiation points with SI less than a threshold are considered to avoid identification of stable locations on downslope paths that do not contain any unstable locations. We evaluate the benefits of this method and the sensitivity to varying the grid size resolution of the DTM used for mapping landslide areas with this method. The MLIP approach was applied to a Stability Index (SI) field obtained from SINMAP using the default parameters suggested by Pack et al. (1998). Flow paths were determined from the D∞ algorithm introduced by Tarboton (1997) and available as part of the open source TauDEM software (http://www.engineering.usu.edu/dtarb/taudem). A range of SI threshold values were used to define MLIPs. The ratio of the density of MLIPs inside and outside mapped landslide areas was used to quantify the ability of the terrain stability map to discriminate terrain instability. High values of the MLIP density ratio indicate good model performance. This approach was applied to a study area located in Northern Region of Italy where landslide runout areas had been mapped from high resolution aerial photographs. The broad question that we address is: What is the influence of high resolution LIDAR derived DTM on terrain stability mapping? Specifically we examined what additional information is obtained from the MLIP method with respect to the standard approach for mapping landslides based on a stability index, and how sensitive is the MLIP method to the DTM grid resolution?

The paper is divided into six sections. In Sect. 2 we define Most Likely Initiation Points (MLIP). Section 3 describes the field area in Northern of Italy where the approach was tested. Section 4 describes the method used to calculate the density of MLIP points within mapped landslide runout zones used to evaluate the model. Section 5 discusses the results and in section 6 we conclude with a summary of our findings.

2 Most Likely Initiation Point definition

A Most Likely Initiation Points (MLIP) is defined as the point along each flow path that has minimum value of Stability Index (SI), corresponding to the most unstable location along the flow path. This is illustrated in Fig. 1 using a terrain stability index map obtained from SINMAP. Figure 1a is shows four flow paths from ridge top to valley and along each path the grid cell with lowest SI is identified. In Fig. 1b the MLIPs along all flow lines are identified. The procedure for evaluation of MLIP consists of first identifying the lowest SI downslope of each point. This is referred to as the minimum downslope value. Then the lowest SI value upslope of each point, the minimum upslope value, is identified. Third the minimum downslope and minimum upslope grids are intersected and where they equal the SI value at the grid cell a MLIP has been identified.

3 Study Area

3.1 Setting

The study area is the Miozza catchment, located in Carnia (a tectonically active area), an alpine region of north-eastern Italy (Fig. 2). The area of the Miozza basin is 10.7 km^2. Elevation ranges from 471 to 2075 m a.s.l. with an average value of 1244 m a.s.l. The slope angle has an average value of 33° with a maximum value of 77°. The only significant human activity in the basin is forestry. The area has a typical North Eastern Alpine climate with short dry periods and a mean annual rainfall of about 2200 mm. Recorded annual rainfall ranges from 1300 to 2500 mm. Precipitation occurs mainly as snowfall from November to April; runoff is usually dominated by snowmelt in May and June. During summer flash floods with heavy solid transport are common. Vegetation covers 94% of the area and consists of forest stands (74%), shrubs (10%) and mountain grassland (10%); the remaining 6% of the area is bedrock

outcrops and unvegetated landslide scars and deposits. The geomorphologic setting of the basin is typical of the eastern alpine region, with deeply incised valleys. Soil thickness varies between 0.2 m and 0.5 m on topographic spurs to depths of up 1.5 m in topographic hollows. The Miozza basin was chosen as a study area because it is representative of the lithological and physiographical conditions frequently observed in the Carnia region where mapping landslide impacts is of interest, and because detailed topographic, land use and geomorphologic information from various sources (including LIDAR) is available. Meteorological data are also available from the regional weather service. Within the study area the area of erosion and shallow landslide scars amounts to 0.5 km^2, i.e. about 4.6% of the total catchment area. The average slope of the landslide scar area is 39°. Most of these areas, in particular the largest single landslide area (0.22 km^2), are located at the head of the basin and occur in complexes (Fig. 3) that result from the aggregation of many shallow landslides.

3.2 Data

Aerial photography, at a resolution of 0.5 m, and field mapping was used to develop a detailed inventory of sediment source, erosion and landslide scars within the study area as illustrated in Figs. 2 and 3. The most recent aerial photographs obtained in Autumn 2004 were used to identify recent landslides not present in earlier surveys. The landslides identified in the aerial photographs were checked in the field.

LIDAR data was collected during snow free conditions in November 2003. The LIDAR survey specifications are listed in Table 1. LIDAR returns were filtered into returns from vegetation and bare ground resulting in an irregular density of ground returns with an average point density of 0.26 points per m^2 (3.8 m^2 per point). Figure 4 illustrates the distribution of bare ground LIDAR elevation points which contains occasional coverage gaps, 5–7 m in extent, in regions of dense vegetation.

HESSD
3, 395–425, 2006

4 Methods

Figure 5 illustrates the steps taken in processing the data to map terrain stability index, SI, and MLIP. The numbers in the description that follow correspond to elements on the flowchart. The bare ground LIDAR data (1) consists of a set of elevation data points (2). These are used as input to the ArcGIS TOPOGRID (3) function to interpolate a DTM (4) with specified grid cell size. The ArcGIS TOPOGRID interpolation function was chosen because it implements a spline algorithm that has been adapted to retain proper topographic characteristics (Hutchinson, 1988, 1989). The DTM grids are used as input to the TauDEM D∞ function (5) that calculates the terrain flow direction (6) and slope (7) grids. The TauDEM Area D∞ function (8) is then used to calculate the specific catchment area (9). Specific catchment area and slope are the terrain inputs to SINMAP (11). SINMAP also takes as input geotechnical and hydrologic parameters (10) characterizing the physical properties of the study area. SINMAP produces a map of the terrain stability index, SI (12). The SI map together with flow direction grid serve as the inputs to the Path Minimum function (13) that evaluates the minimum SI value upslope of (14) and downslope from (15) each grid cell. The minimum upslope and downslope grids, in combination with the SI grid are used to determine the MLIP grid (16). Details of SINMAP and the algorithm for evaluation of MLIP are given below.

Once SI and MLIP have been derived they are compared to the observed landslide areas using density ratios. SINMAP was used to derive a map of SI for each resolution DTM grid. MLIPs were mapped for each DTM grid and a range of SI threshold values. For each SI map corresponding to each DTM grid resolution and a range of SI thresholds we counted the number of grid cells within and outside the mapped landslide area with SI less than the threshold value. This was used to determine the SI density ratio using the following equation

$$\text{density ratio of SI} = \frac{(\text{SI}_{\text{lds}}/\text{landslide area})}{(\text{SI}_{\text{bas}}/\text{basin area})} \quad (1)$$

where SI_{lds} is the number of SI cells less than the threshold that falls within the landslide

area and SI_{bas} is the total number of grid cells with SI less than the threshold within the basin. For the MLIP map corresponding to each DTM resolution and SI threshold we counted the number of grid cells within and outside the mapped landslide area. This was used to determine the MLIP density ratio using the following equation

$$\text{density ratio of MLIP} = \frac{(P_{lds}/\text{landslide area})}{(P_{bas}/\text{basin area})} \quad (2)$$

where P_{lds} and P_{bas} are respectively the number of MLIP grid cells within the landslide area and within the basin as a whole. The density ratios calculated using this procedure were used to compare SI and MLIP maps developed using different DTM resolutions and SI threshold, S_{thr}. High values of the density ratio correspond to better performance of the model in discriminating areas where landslides have been observed.

4.1 Stability index

SINMAP (Pack et al., 1998) is based upon the infinite slope stability model (e.g. Hammond et al., 1992; Montgomery and Dietrich, 1994) that balances the destabilizing components of gravity and the restoring components of friction and cohesion on a failure plane parallel to the ground surface with edge effects neglected (Fig. 6). The infinite slope stability model factor of safety (ratio of stabilizing to destabilizing forces) used in SINMAP is given by the following equation

$$FS = \frac{C + \cos\theta \left[1 - \min\left(\frac{R}{T}\frac{a}{\sin\theta}, 1\right) r\right] \tan\phi}{\sin\theta} \quad (3)$$

where C is dimensionless cohesion, r is the ratio of the density of water to the density of soil (ρ_w/ρ_s), θ is slope angle, ϕ the internal friction angle and $\min\left(\frac{R}{T}\frac{a}{\sin\theta}, 1\right)$ is an estimate of the relative wetness derived following TOPMODEL assumptions (Beven and Kirkby, 1979) of steady state drainage driven by a topographic gradient. Dimensionless cohesion, C, is defined as $(C_r+C_s)/(h\rho_s g)$, where C_r and C_s are root strength and soil cohesion terms, h is the thickness of the soil (Fig. 6) and g the gravitational

constant. In the expression for relative wetness, a (m) is the specific catchment area derived from the DTM (Tarboton, 1997), T is soil transmissivity (m^2/hr), and R is steady state recharge (m/hr).

In Eq. (3) a and θ are derived from the DTM. SINMAP takes the geophysical parameters C, R/T and $\tan\phi$ as uncertain and assumes that each has a uniform probability distribution. The stability index (SI) is defined with respect to these probability distributions as the probability that a location is stable, i.e. has FS>1 (Pack et al., 1998).

$$\text{SI} = \text{Prob}(\text{FS} > 1) \tag{4}$$

In the special case that FS is greater than 1 for all values of C, R/T and $\tan\phi$ within their uniform distribution ranges SI is reported as the FS value for the most conservative parameter values, namely the minimum C and $\tan\phi$ and maximum R/T.

With the physical parameters being taken as uncertain, the parameters input to SINMAP become the minimum and maximum values of the ranges that define the uniform probability distributions. In SINMAP T/R is used as an input parameter rather than R/T because it has a physical interpretation as the hillslope length required for saturation under parallel flow conditions.

4.2 Calculation of MLIP

The numerical evaluation of MLIP is achieved in three steps. First minimum values downslope of, and upslope from, each grid cell are computed. These are then combined with the original SI grid to evaluate MLIP locations. This procedure was followed so as to take advantage of the efficiency provided by a recursive evaluation of minimum downslope and minimum upslope values adapted from the recursive evaluation of contributing area used by Tarboton (1997) with the D∞ multiple flow direction model for representation of flow over a terrain surface.

Figure 7 illustrates the minimum upslope function. Figure 7a is an example of a SI grid. Figure 7b gives a flow path through this grid. The values of the minimum upslope function along this flow path are given in Fig. 7c. On this flow path the top left grid

cell has no grid cells upslope, so is regarded as a ridge top grid cell and is assigned a minimum upslope value equal to the cell value itself (in this case 0.8). Moving one cell down the flow path the minimum upslope value is the minimum of 0.8 and 0.7 so the second cell along the flow path is assigned a minimum upslope value of 0.7. Similarly the middle grid cell is assigned a minimum upslope value of 0.1, the minimum of 0.8, 0.7 and 0.1. The fourth grid cell has a SI value of 0.5, but the minimum upslope value is assigned as 0.1, the minimum of 0.8, 0.7, 0.1 and 0.5. Similarly the last grid cell on the flow path is assigned a minimum upslope value of 0.1, the minimum of 0.8, 0.7, 0.1, 0.5 and 0.8. Numerically the minimum upslope value is computed recursively as the minimum of the cell value itself and the result from the minimum upslope function applied at grid cells immediately upslope. In other words, instead of the minimums of multiple grid cells described above at the third cell the evaluation is the minimum of the cell value of 0.1 and the minimum upslope from the second grid cell, 0.7. At the fourth cell the evaluation is the minimum of the cell value of 0.5 and the minimum upslope of the third grid cell, 0.1, and so on. In general there may be multiple grid cells immediately upslope of any specific grid cell, because flow paths merge. Furthermore in the D∞ approach the flow between grid cells is proportioned according to the flow direction angle. Only a fraction of the flow from each upslope grid cell contributes to a downslope grid cell. When identifying minimum values along a flow path the question arises as to what fraction of flow should be considered for the flow path to be "counted". We (arbitrarily) selected a proportion of 0.2 (20%). Grid cells that contribute 20% or more of their flow to a grid cell are counted as being upslope of a grid cell for the purposes of evaluating the minimum upslope grid value. The procedure was implemented in a C++ computer program.

Figure 8 illustrates the minimum downslope function, the computation of which is similar to the minimum upslope function except that instead of looking at each grid cell upslope from a specific grid cell it looks at each grid cell downslope from a specific grid cell.

The minimum upslope and minimum downslope grids are evaluated separately be-

cause recursion can not function in the upslope and downslope directions simultaneously. However once the minimum upslope and downslope grids have been evaluated the minimum value along a flow path can be identified by the condition that the minimum upslope value is equal to the minimum downslope value and the value at the grid cell itself. This is illustrated in Fig. 9. The MLIP method can be used without any condition on the values of SI at the MLIP location. However, some flow paths that never go through an unstable location will still be identified as MLIP because they have the lowest SI value along the flow path, but the SI value may be large and unlikely to be a landslide initiation point. Therefore we use a threshold with the identification of MLIP points, only identifying MLIP locations whose SI value is less than the input threshold SI_{thr}. In the illustration in Fig. 9, SI_{thr}=0.2 results in identification of only the dark grid cells as MLIP locations.

5 Results and discussion

Five digital terrain models (DTMs) were interpolated for the study area with progressively finer grid cell resolutions of 50, 20, 10, 5 and 2 m. For each of these DTMs SINMAP was used to map stability index, SI, using default parameters: 0-0.25 for the range of dimensionless cohesion, 30°–45° for the range of internal frictional angle, and 2000–3000 m for the range of the ratio T/R . The observed landslides were overlaid on each of these SI maps and for stability index thresholds of 0.2, 0.5, 1 and 10 the percentage of area with SI less than the threshold and density ratio of SI less than the threshold was calculated using Eq. (1). The results are given in Tables 2 and 3. Based on the SI maps for each DTM grid resolution MLIP locations were identified using the procedure described above for stability index thresholds, SI_{thr} of 0.2, 0.5, 1, and 10 again. For each of these MLIP maps the percentage of MLIP locations occurring within the mapped landslide area and the density ratio of MLIP locations identified was calculated using Eq. (2). The results are also given in Tables 2 and 3.

These tables allow us to assess the effectiveness of the SI map and MLIP proce-

dure at discriminating potential landslide initiation locations in comparison to mapped landslide locations. We see in Table 2 that as the SI threshold is reduced the percentage of terrain less than the SI threshold that falls within the mapped landslide scars increases, reflecting the general effectiveness of the SI approach. The trend is essentially the same for all grid resolutions. In Table 3 the density ratio values indicate that at the lowest SI threshold the ratio of density between points within and outside landslide scars is around 2.5, a measure of the effectiveness of simple SI thresholding at discriminating landslide scars locations. However, as mentioned before this comparison is hampered by the fact that mapped landslides included the entire landslide scar, not only the initiation zones.

The MLIP results in Tables 2 and 3 allow us to assess the effectiveness of the MLIP locations identified from the SI map. Notable in these tables are that the MLIP percentages and ratios are (in 18 out of 20 cases) higher than SI percentages and ratios. Also the percentages remain similar across SI_{thr} values. This is the result of the MLIP procedure identifying the lowest SI value along a flow path and this lowest value frequently being within the mapped landslide scar regardless of threshold. In Table 3, the density ratios of MLIP are generally higher than SI, with values as high as 3.8, indicating that in this setting where mapped landslides include the entire landslide scar the MLIP procedure is more effective at quantifying the effectiveness of the SI map at discriminating potential landslide initiation locations.

It is also of interest to note that the highest MLIP percentage and density ratios occur for a DTM grid cell resolution of 10 m, with the one exception of the smallest threshold and largest DTM cell size. This is a small sample effect that we disregard. With a 50 m cell size and 0.2 threshold there are only 20 MLIP grid cells, insufficient to be representative. The peak in MLIP density ratios for DTM grid cell resolution of 10 m we take as support for the idea that a 10 m DTM grid cell resolution is optimal for the identification of potential instability in terrain stability mapping. This may be a natural scale associated with the landslides under consideration. At scales coarser than 10 m the loss of information appears to result in a drop off in the discriminating

capability of the SI map as quantified by MLIP density ratio. At scales finer than 10 m small scale errors in the determination of slope, for example, may result in increases in the number of spurious MLIP locations reducing the discriminating capability. It is also worth noting with respect to this issue that the convergence of subsurface flow that is quantified by the DTM computed specific catchment area is a process that is more likely to be influenced by the larger scale topographic slope than small surface irregularities represented by a very high resolution DTM. This may be another reason for the optimal discriminating capability of a 10 m resolution DTM in this study. There is also a small slope scale effect bias that impacts the results. For the 50 m resolution DTM the mean slope is 28°, while for the 2 m resolution DTM the mean slope is 33°.

Figure 10 gives the MLIP map for the study area with SI_{thr}=1, compared to mapped landslide scars. Note in this figure how MLIP locations cluster at the upslope end of landslide scars indicating their most likely initiation points. Figure 11 illustrates the mapped MLIP locations draped on an aerial photograph of part of the study area. Figure 12 illustrates MLIP for end members of the DTM resolution range for one landslide complex, showing these scale effects. At the 50 m resolution the DTM is too coarse to resolve the detail in the landslide scar. At 2 m resolution the MLIP locations spread out as a blur, rather than a line of single MLIP locations such as generally the case in Fig. 10.

6 Conclusions

The Most Likely Initiation Point (MLIP) method has been introduced as a new way to generate information from terrain stability maps. MLIP locations are of interest because they identify the most potentially unstable location along each flow path. They also provide a way to assess the discriminating capability of a terrain stability map in comparison to mapped landslide scars. This discriminating capability was measured using the ratio of the density of MLIP locations within and outside mapped landslide scars. MLIP locations proved to have a greater discriminating capability than simple

thresholding of the SI map in the study area where this was applied where mapped landslide scars include runout areas. In this work we made no effort to calibrate or adjust the parameters of the terrain stability model (SINMAP); rather default model parameter were used. This was done to evaluate the generality of the MLIP approach and given the ratios in excess of 3 of MLIP density between within landslide and outside of landslide area we believe that the MLIP approach has generality beyond our specific study area. The comparisons of MLIP density ratios for different resolution DTMs showed that for this data a 10 m resolution DTM is optimal. Future work should test this approach in other settings and with other terrain stability models, such SHALSTAB (Montgomery and Dietrich, 1994) and Borga et al.'s (2002), quasi dynamic model.

Acknowledgements. This research was supported by the Interreg IIIB Spazioalpino project: CATCHRISK (Mitigation of hydrogeological risk in alpine catchments). The authors are grateful to "Servizio Territorio Montano e Manutenzioni" (Direzione Centrale Risorse Agricole, Naturali, Forestali e Montagna) of Friuli Venezia Giulia Region for the collaboration in field surveys and providing aerial photography data. LIDAR data were collected in the Interreg IIIA Italia-Slovenia project: "Ricomposizione della cartografia catastale e integrazione della cartografia regionale numerica per i sistemi informativi territoriali degli enti locali mediante sperimentazione di nuove tecniche di rilevamento". This work has benefited from discussion with K. Chinnayakanahalli. P. Tarolli also acknowledges the contributions of G. Dalla Fontana and M. Borga during the prework discussion, and the support of Ing. Aldo Gini Foundation on the scholarship period at Utah State University.

References

Ackermann, F.: Airborne laser scanning – present status and future expectations, IS-PRN Journal of Photogrammetry and Remote Sensing, 54, 64–67, 1999.

Borga, M., Dalla Fontana, G., and Cazorzi, F.: Analysis of topographic and climatic control on rainfall-triggered shallow landsliding using a quasi-dynamic wetness index, J. Hydrol., 268(1–4), 56–71, 2002.

Briese, C.: Breakline Modelling from Airborne Laser Scanner Data, PHD thesis, Institute of Photogrammetry and Remote Sensing, Vienna University of Technology, 2004.
Dietrich, W. E., Wilson, C. J., Montgomery, D. R., McKean, J., and Bauer, R.: Erosion Thresholds and Land Surface Morphology, Geology, 20, 675–679, 1992.
Hammond, C., Hall, D., Miller, S., and Swetik, P.: Level I Stability Analysis (LISA) Documentation for Version 2.0," General Technical Report INT-285, USDA Forest Service Intermountain Research Station, 1992.
Hutchinson, M. F.: Calculation of hydrologically sound digital elevation models, Third International Symposium on Spatial Data Handling, Sydney, Columbus, Ohio, International Geographical Union, 1988.
Hutchinson, M. F.: A new procedure for gridding elevation and stream line data with automatic removal of spurious pits, J. Hydrol., 106, 211–232, 1989.
Kraus, K. and Pfeifer, N.: Advanced DTM generation from LIDAR data, International Archives of Photogrammetry and Remote Sensing, XXXIV-3/W4, 23–35, 2001.
McKean, J. and Roering, J.: Objective landslide detection and surface morphology mapping using high-resolution airborne laser altimetry, Geomorphology, 57, 331–351, 2004.
Montgomery, D. R. and Dietrich, W. E.: A physically based model for the topographic control on shallow landsliding, Water Resour. Res., 30(4), 1153–1171, 1994.
Pack, R. T., Tarboton, D. G., and Goodwin, C. N.: The SINMAP Approach to Terrain Stability Mapping, 8th Congress of the International Association of Engineering Geology, Vancouver, British Columbia, Canada, 1998.
Tarboton, D. G.: A new method for the determination of flow directions and upslope areas in grid digital elevation models, Water Resour. Res., 33, 309–319, 1997.
Wu, W. and Sidle, R. C.: A Distributed Slope Stability Model for Steep Forested Watersheds, Water Resour. Res., 31(8), 2097–2110, 1995.

Table 1. LIDAR data specifications for Miozza cacthment survey.

Technique	helicopter laserscan
Fly	strips
Instrument	ALTM 3033 OPTECH
Flying height	1000 m a.g.l. (above ground level)
Flying speed	80 kts
Scan angle	20°
Scan rate	33 KHz
Point density	mean >1 points per m^2 (2.5 per m^2) with "*first & last pulses*"

HESSD
3, 395–425, 2006

Table 2. Percentage of area with SI less than threshold, and percentage of identified MLIP locations occurring within mapped landslide area.

Grid resolution (m)	50		20		10		5		2	
SI thresholds	SI	**MLIP**	SI	**MLIP**	SI	**MLIP**	SI	**MLIP**	SI	**MLIP**
SI<0.2	16.3	**25.0**	11.8	**8.7**	12.5	**18.2**	11.2	**14.2**	11.2	**12.28**
SI<0.5	10.7	**15.3**	10.9	**9.2**	10.7	**17.5**	10.7	**14.0**	10.4	**12.27**
SI<1	6.4	**7.3**	6.1	**6.8**	6.2	**16.9**	6.2	**13.9**	6.3	**12.27**
SI<10	4.7	**7.0**	4.7	**6.6**	4.7	**16.8**	4.7	**13.9**	4.7	**12.26**

HESSD
3, 395–425, 2006

P. Tarolli and
D. G. Tarboton

EGU

Table 3. Density ratio between locations with SI less than a threshold, and between MLIP locations, within and outside the observed landslide area.

Grid resolution (m)	50		20		10		5		2	
SI thresholds	SI	**MLIP**	SI	**MLIP**	SI	**MLIP**	SI	**MLIP**	SI	**MLIP**
SI<0.2	3.41	**5.23**	2.47	**1.83**	2.61	**3.81**	2.35	**2.97**	2.34	**2.57**
SI<0.5	2.25	**3.19**	2.27	**1.91**	2.23	**3.66**	2.24	**2.93**	2.17	**2.57**
SI<1	1.33	**1.53**	1.27	**1.42**	1.29	**3.53**	1.29	**2.91**	1.31	**2.57**
SI<10	1	**1.46**	1	**1.38**	1	**3.51**	1	**2.91**	1	**2.56**

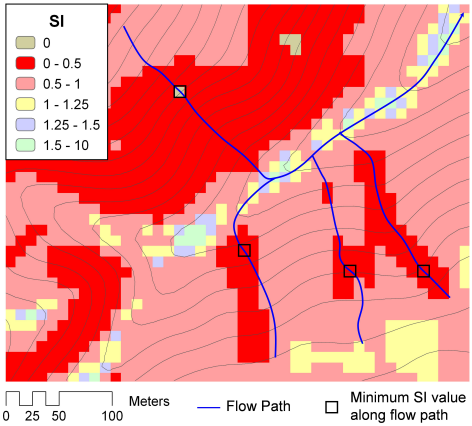

(a)

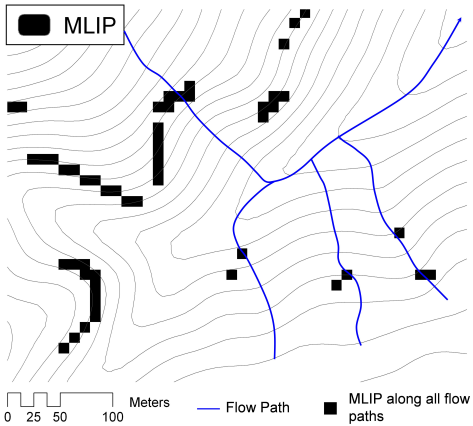

(b)

Fig. 1. Illustration of Most Likely Initiation Points (MLIP). **(a)** SINMAP Stability Index (SI) map with the locations of the lowest SI value along four example flow paths identified. **(b)** MLIP locations identified for all flow paths.

HESSD
3, 395–425, 2006

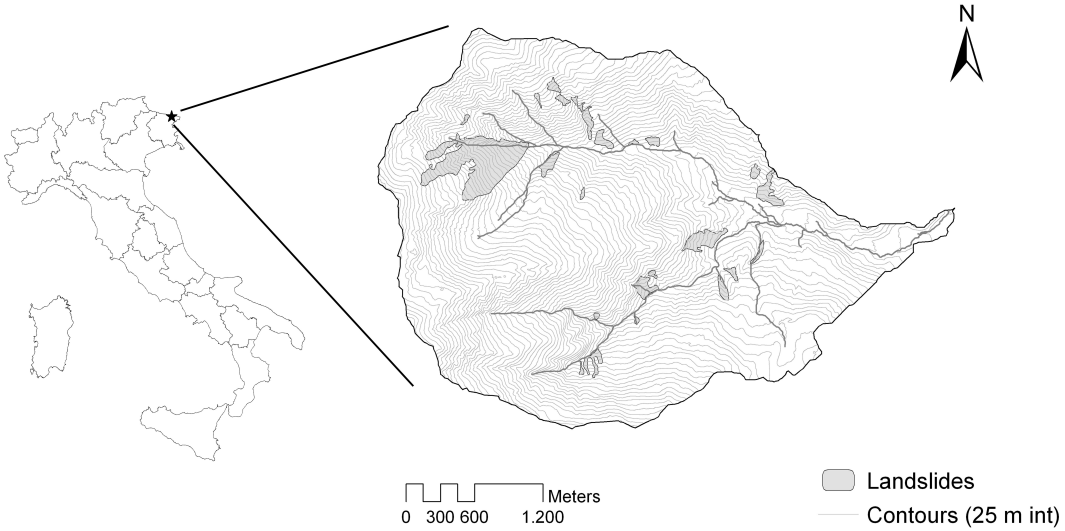

Fig. 2. Miozza basin location map.

HESSD
3, 395–425, 2006

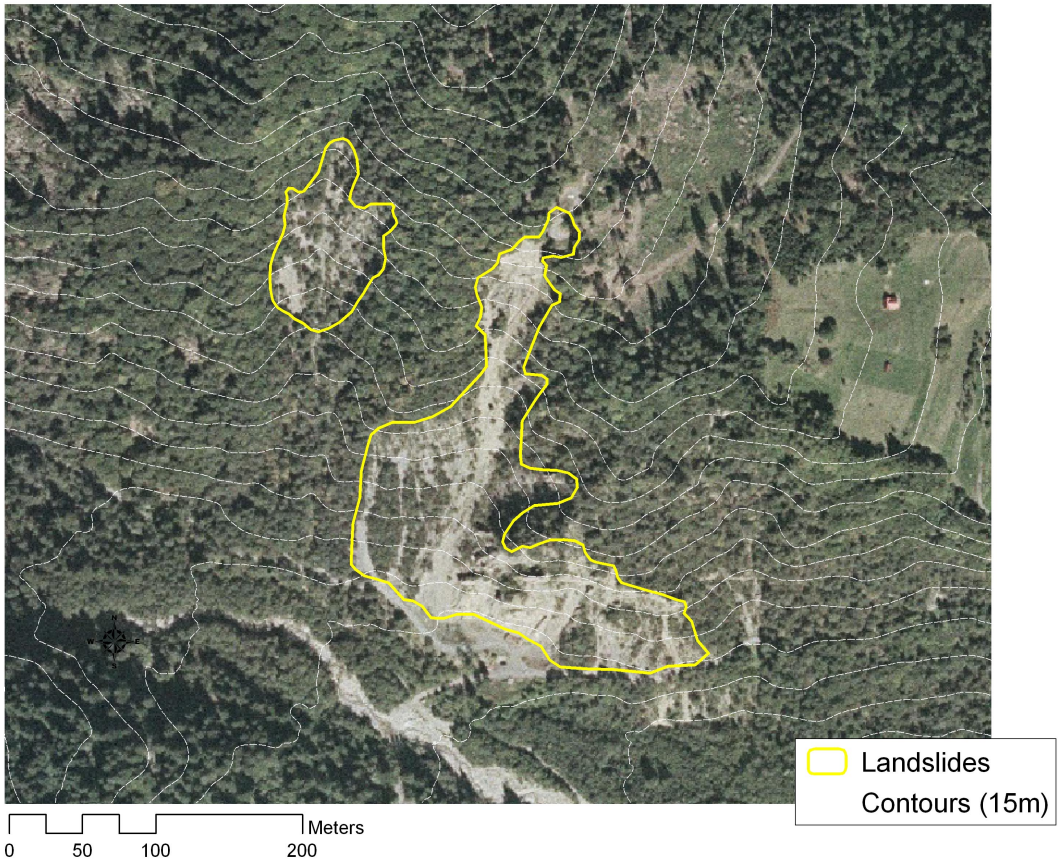

Fig. 3. Miozza basin landslide scars identified from aerial photography: illustration of a landslide complex.

HESSD
3, 395–425, 2006

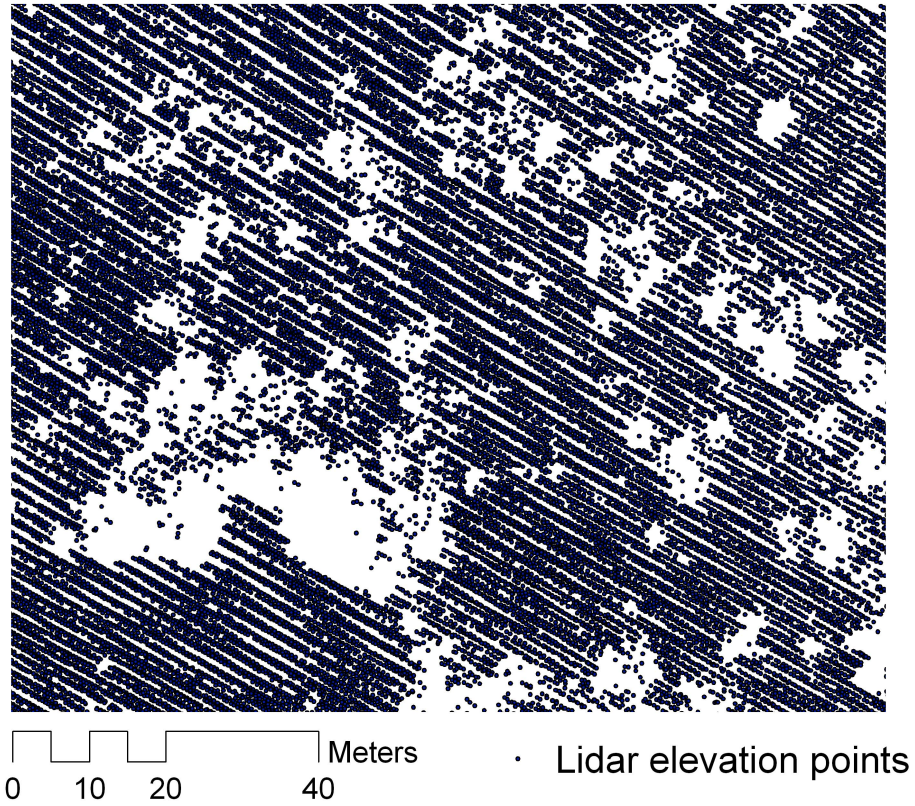

Fig. 4. Illustration of the irregular distribution of filtered LIDAR bare ground elevation points.

HESSD
3, 395–425, 2006

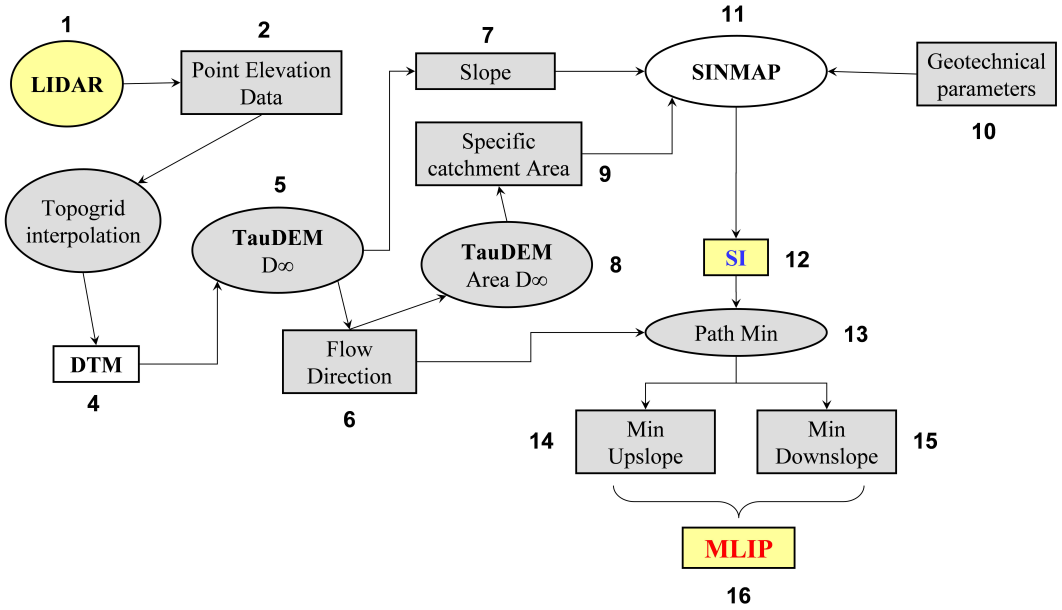

Fig. 5. MLIP model flow diagram.

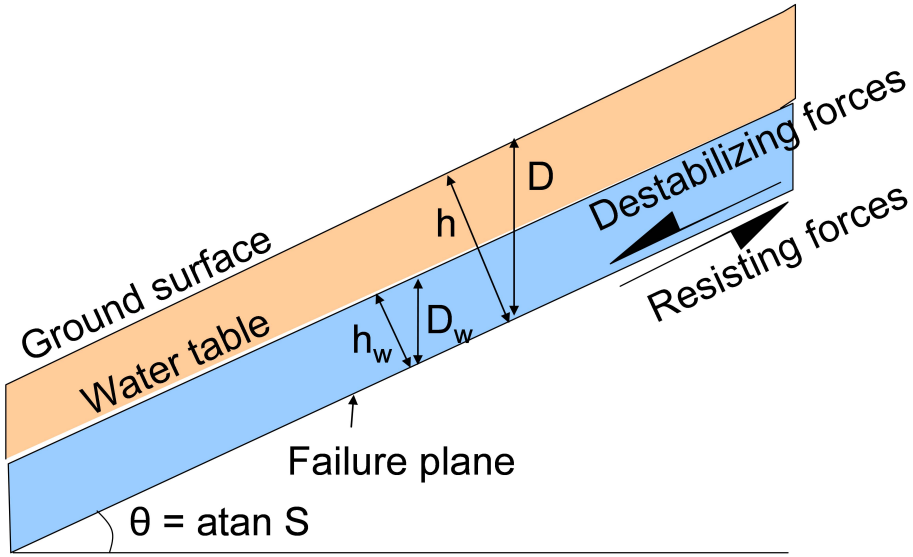

Fig. 6. Infinite slope stability model schematic.

HESSD
3, 395–425, 2006

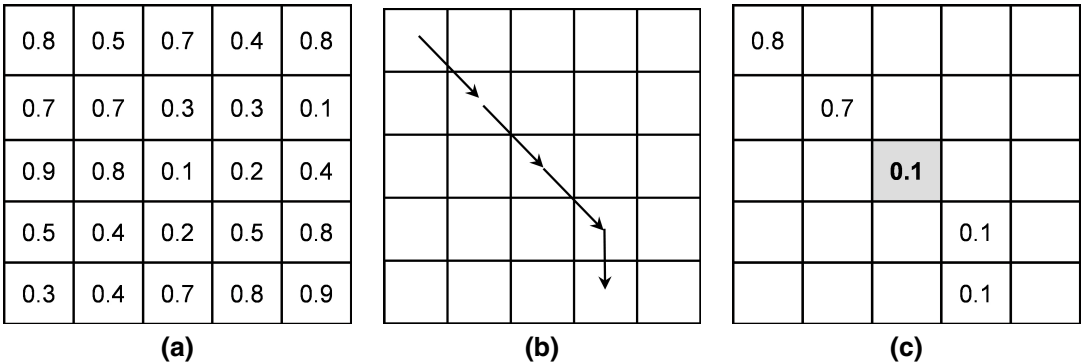

Fig. 7. Illustration of the minimum upslope function. **(a)** Example SI grid. **(b)** Example flow path. **(c)** Example values of the minimum upslope function along the flow path in (b).

HESSD
3, 395–425, 2006

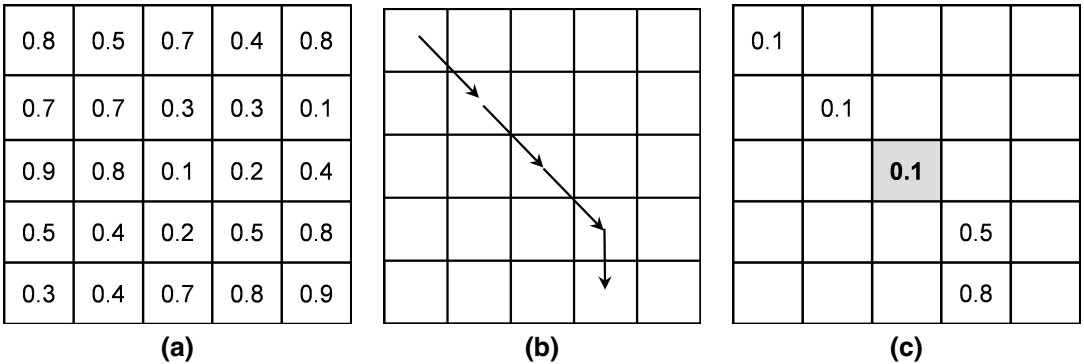

Fig. 8. Illustration of the minimum downslope function. **(a)** Example SI grid. **(b)** Example flow path. **(c)** Example values of the minimum downslope function along the flow path in (b).

HESSD
3, 395–425, 2006

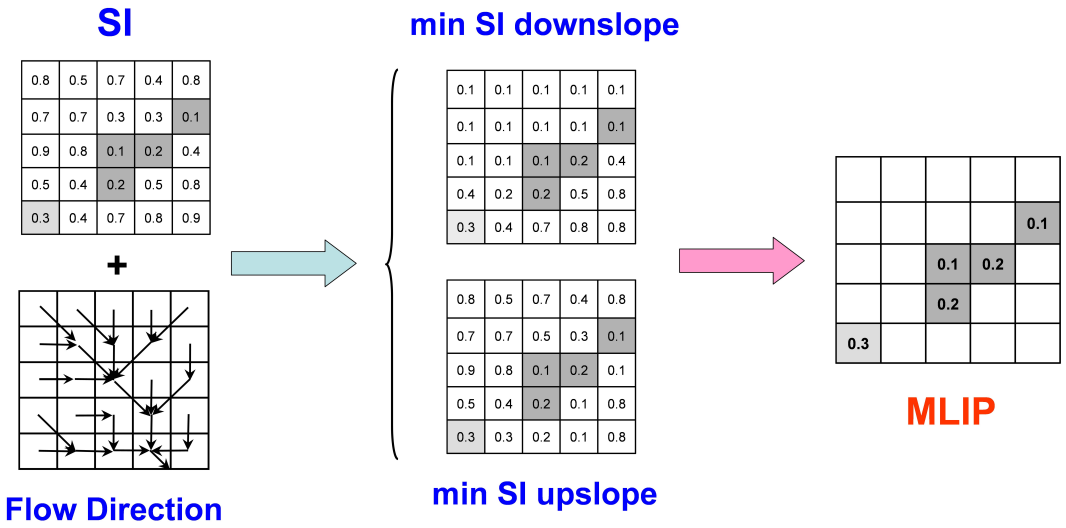

Fig. 9. Illustration of the combination of minimum upslope and minimum downslope functions to identify Most Likely Initiation Points (MLIP). The shaded grid cells are identified as MLIP in all cases. The dark shaded grid cells are MLIP determined for $SI \leq SI_{thr}=0.2$.

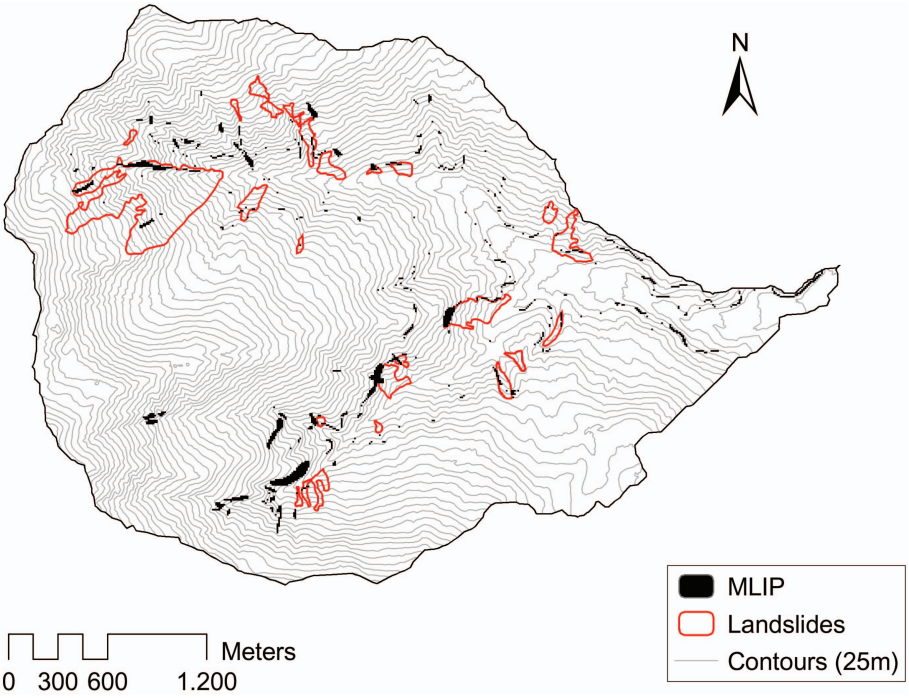

Fig. 10. MLIP map for 10 m resolution DTM grid and $SI_{thr}<1$.

HESSD
3, 395–425, 2006

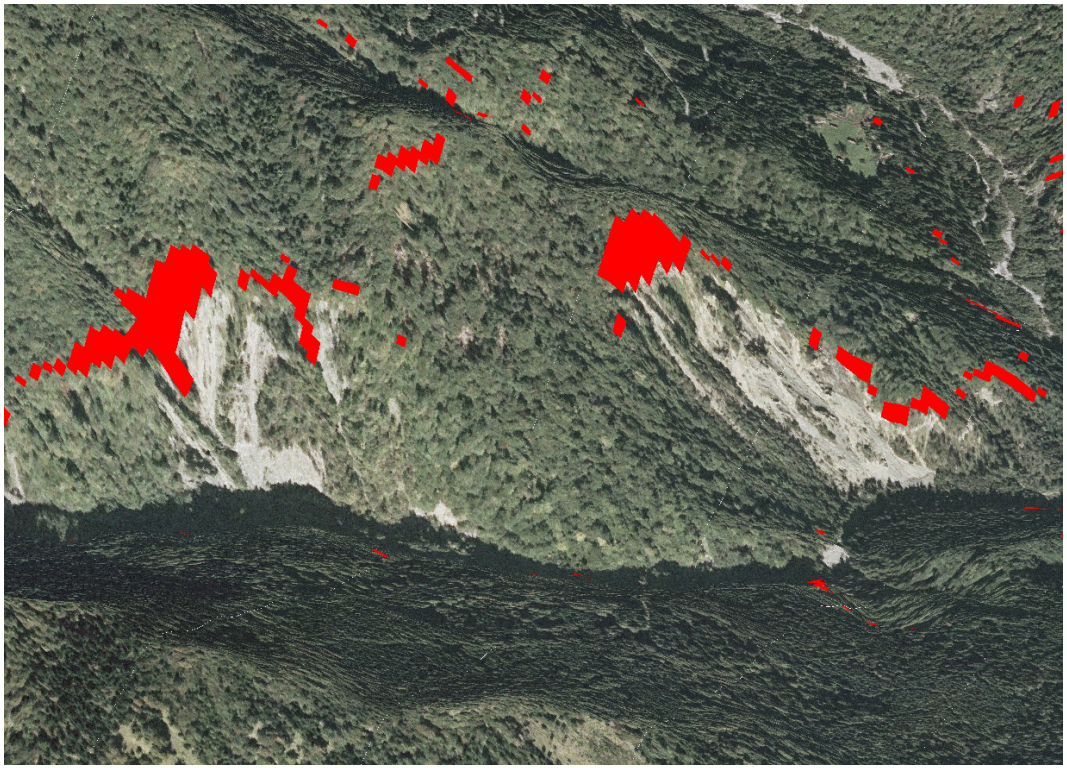

Fig. 11. 3-D view of MLIP locations.

HESSD

3, 395–425, 2006

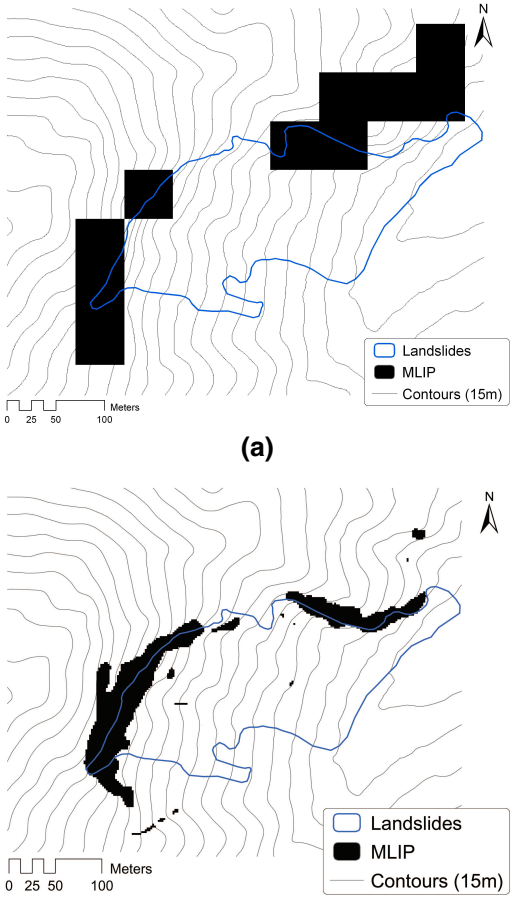

Fig. 12. Illustration of MLIP locations identified (without SI threshold) for one landslide complex for endpoints in the range of DTM resolutions used: **(a)** 50 m DTM resolution **(b)** 2 m DTM resolution.

HESSD
3, 395–425, 2006